

Cross-Disease Comparison of Amyotrophic Lateral Sclerosis and Spinal Muscular Atrophy Reveals Conservation of Selective Vulnerability but Differential Neuromuscular Junction Pathology

Laura H. Comley,* Jik Nijssen, Johanna Frost-Nylen, and Eva Hedlund*

Department of Neuroscience, Karolinska Institutet, Stockholm, Sweden

Neuromuscular junctions are primary pathological targets in the lethal motor neuron diseases spinal muscular atrophy (SMA) and amyotrophic lateral sclerosis (ALS). Synaptic pathology and denervation of target muscle fibers has been reported prior to the appearance of clinical symptoms in mouse models of both diseases, suggesting that neuromuscular junctions are highly vulnerable from the very early stages, and are a key target for therapeutic intervention. Here we examined neuromuscular pathology longitudinally in three clinically relevant muscle groups in mouse models of ALS and SMA in order to assess their relative vulnerabilities. We show for the first time that neuromuscular junctions of the extraocular muscles (responsible for the control of eye movement) were resistant to degeneration in end-stage SMA mice, as well as in late symptomatic ALS mice. Tongue muscle neuromuscular junctions were also spared

in both animal models. Conversely, neuromuscular junctions of the lumbrical muscles of the hind-paw were vulnerable in both SMA and ALS, with a loss of neuronal innervation and shrinkage of motor endplates in both diseases. Thus, the pattern of selective vulnerability was conserved across these two models of motor neuron disease. However, the first evidence of neuromuscular pathology occurred at different timepoints of disease progression, with much earlier evidence of presynaptic involvement in ALS, progressing to changes on the postsynaptic side. Conversely, in SMA changes appeared concomitantly at the neuromuscular junction, suggesting that mechanisms of neuromuscular disruption are distinct in these diseases. *J. Comp. Neurol.* 524:1424–1442, 2016.

© 2015 The Authors The Journal of Comparative Neurology Published by Wiley Periodicals, Inc.

INDEXING TERMS: extraocular; tongue; lumbricals; oculomotor; SOD1; SMN

Amyotrophic lateral sclerosis (ALS) and spinal muscular atrophy (SMA) are characterized by the loss of somatic motor neurons and innervation to voluntary skeletal muscles, leading to death by respiratory failure. There is currently no cure for either disease. ALS is the most common form of motor neuron disease, with a life-time risk of 1:300 (Al-Chalabi et al., 2012). It is typically adult-onset and very aggressive, with most patients dying 2–3 years after diagnosis. ALS appears sporadic in 90% of cases, but can also be inherited. Mutations in multiple different genes are disease-causative including *superoxide dismutase 1 (SOD1)*, *TARDBP (TDP43)*, *Fused in sarcoma (FUS)* and *Chromosome 9 open reading frame 72 (C9ORF72)* (Renton et al., 2014). SMA is an autosomal recessive disease, with onset occurring before

This is an open access article under the terms of the Creative Commons Attribution-NonCommercial-NoDerivs License, which permits use and distribution in any medium, provided the original work is properly cited, the use is non-commercial and no modifications or adaptations are made. Grant sponsor: EU Joint Programme for Neurodegenerative Disease (JPND); Grant sponsor: Ragnar Söderbergs Stiftelse; Grant number: M245/11; Grant sponsor: Swedish Medical Research Council (Vetenskapsrådet); Grant number: 2011-2651; Grant sponsor: Birgit Backmark Donation to ALS research; Grant sponsor: Stiftelsen Olle Engkvist Byggmästare; Grant number: 2014/204; Grant sponsor: Karolinska Institutet Fonder; Grant sponsor: Åhlén-stiftelsen; Grant numbers: mB8/h11; mB8/h12; mB8/h13; mB8/14; Grant sponsor: Prinses Beatrix Spierfonds; Grant number: W.S14-06.

*CORRESPONDENCE TO: L. Comley or E. Hedlund, Department of Neuroscience, Karolinska Institutet, Retzius v. 8, 171 77 Stockholm, Sweden. E-mail: laura.comley@ki.se or eva.hedlund@ki.se

Received June 15, 2015; Revised October 16, 2015;

Accepted October 22, 2015.

DOI 10.1002/cne.23917

Published online November 23, 2015 in Wiley Online Library (wileyonlinelibrary.com)

The copyright line for this article was changed on December 7 after original online publication.

© 2015 The Authors The Journal of Comparative Neurology Published by Wiley Periodicals, Inc.

6 months and lethality by 2 years of age in its most severe form. SMA is the most common genetic cause of infant mortality, with an annual incidence of 1:6,000–1:10,000 live births and a carrier frequency of ~1:40 (Faravelli et al., 2015). SMA is caused by mutations in the *survival motor neuron 1 (SMN1)* gene leading to low levels of SMN protein (Coovert et al., 1997). Despite the differing genetic triggers, a principle early feature of both ALS and SMA is the loss of contact between nerve and muscle, which occurs at a specialized synapse called the neuromuscular junction. Pathology then progresses in a distal to proximal direction, known as a “dying-back” pathology (reviewed in Murray et al., 2010). Changes at the neuromuscular junction have been shown to occur before central cell body loss is seen, and before the appearance of clinical symptoms in the SOD1^{G93A} ALS mouse model (Frey et al., 2000; Fischer et al., 2004; Liu et al., 2015). Studies in human ALS patients suggest the same phenotype; morphological changes at the neuromuscular junction in muscle biopsies and alterations in electrophysiological recordings of neuromuscular transmission are some of the earliest signs of disease (Dengler et al., 1990; Maselli et al., 1993; Fischer et al., 2004; Bruneteau et al., 2015). Similarly, early changes at the neuromuscular junction have been reported in several mouse models of SMA (Cifuentes-Diaz et al., 2002; Kariya et al., 2008; Murray et al., 2008; Kong et al., 2009).

While neuromuscular junctions are early pathological targets in both ALS and SMA, each disease has a pattern of vulnerability whereby different motor neurons and their respective muscle groups appear more or less vulnerable to degeneration (Ling et al., 2012; Thomson et al., 2012; Tjust et al., 2012; Valdez et al., 2012). In particular, ocular motor neurons and their targets, the extraocular muscles, which control the movement of the eyes (Gizzi et al., 1992; Nimchinsky et al., 2000; Haenggeli and Kato, 2002), are commonly held to be relatively resistant in motor neuron diseases. In human ALS patients eye movement can be used as a means of communication when many other muscle groups, including those necessary for speech, have been denervated and thus atrophied (Spataro et al., 2014). Studies using mouse models have provided evidence for preservation of the neuromuscular junctions within the extraocular muscles in both ALS and aging (Tjust et al., 2012; Valdez et al., 2012). Evidence for the sparing of extraocular muscles in SMA is sparse. Clinical wisdom and the utility of ocular tracking devices (Kubota et al., 2000) suggest that these muscles are relatively resistant also in this disease.

In ~30% of ALS patients, onset of disease occurs in the bulbar region (Logroscino et al., 2010). However, hypoglossal abnormalities have not been firmly shown in animal models. Early-symptomatic SOD1^{G93A} mice display mild loss of hypoglossal motor neurons, which then progressed by endstage of disease (Haenggeli and Kato,

2002). However, in the SOD1^{G85R} mouse model only very mild hypoglossal motor neuron loss was seen (Nimchinsky et al., 2000). As with the extraocular muscles, the only evidence for hypoglossal involvement in SMA comes from clinical studies, where tongue fasciculations have been described in patients (Iannaccone et al., 1993). Around 60% of ALS cases are diagnosed as “limb onset” (Logroscino et al., 2010). Many seminal studies of neuromuscular pathology in SOD1 ALS mouse models have used hind-limb muscles to demonstrate vulnerability of the neuromuscular system (Bjornskov et al., 1984; Frey et al., 2000; Fischer et al., 2004; Schaefer et al., 2005; Tjust et al., 2012; Valdez et al., 2012). The lumbricals are four small skeletal muscles that aid the flexion of the foot. These muscles are ideal for morphological studies of the neuromuscular junction in mouse models, as their small size allows for the entire innervation pattern to be viewed (Sleigh et al., 2014). Despite this, the relative vulnerability of the lumbrical muscles has not been assessed in mouse models of ALS. In contrast, several studies have analyzed pathology of the lumbricals in SMA mouse models, but with conflicting reports of the severity of denervation, depending on the strain used (Cifuentes-Diaz et al., 2002; Kariya et al., 2008; Murray et al., 2008; Kong et al., 2009; Ling et al., 2012).

Here we examined neuromuscular pathology in the extraocular, tongue, and lumbrical muscles in mouse models of ALS and SMA. We compared presynaptic and postsynaptic pathology of the muscle endplate in these three muscle groups in order to assess their relative vulnerabilities. We analyzed muscles at several timepoints throughout both diseases, from early symptomatic to late symptomatic or endstage in order to gain a thorough understanding of the time course of distal disease pathology. By using both the SOD1^{G93A} mouse model of ALS and the SMN Δ 7 model of SMA we were able to compare and contrast the response of the neuromuscular system to motor neuron diseases with distinct etiologies and genetic triggers.

MATERIALS AND METHODS

Mouse strains

All animal procedures were previously approved by the Swedish ethical council (Stockholms Norra Djurförsöksetiska nämnd), in compliance with US National Institutes of Health guidelines. Animals were housed according to standard conditions, with access to food and water ad libitum and a dark/light cycle of 12 hours. SMN Δ 7 mice were used as a model for SMA (FVB.Cg-Tg(SMN2*delta7)4299AhmbTg(SMN2) 89AhmbSmn1^{tm1Msd}/J; Jackson Laboratory, Bar Harbor, ME, Stock Number 005025; (Le et al., 2005)). These mice are knockout for mouse

TABLE 1.

Number of SMA Mice and Control Littermates Used to Quantify Presynaptic Pathology

Age (postnatal day)	Genotype	Muscle group	N		
			Mice	Muscles	NMJs
P5	Control	Extraocular	3	3	290
		Tongue	4	4	386
		Lumbricals	4	6	497
	SMA	Extraocular	3	3	224
		Tongue	5	5	447
		Lumbricals	3	6	524
P10	Control	Extraocular	4	4	211
		Tongue	5	5	557
		Lumbricals	4	11	1076
	SMA	Extraocular	4	5	404
		Tongue	5	5	504
		Lumbricals	4	9	859
P14	Control	Extraocular	3	4	133
		Tongue	3	3	358
		Lumbricals	3	5	357
	SMA	Extraocular	3	4	393
		Tongue	4	4	463
		Lumbricals	3	5	575

Smn1 but express a single copy of human *SMN2* and a second transgene with a human *SMN2* promoter regulating expression of human *SMN2* cDNA that lacks exon 7 (*Smn*^{-/-}; *SMN2*; *SMNΔ7*). Littermates both homozygous and heterozygous for *Smn1* were previously shown to be indistinguishable (Monani et al., 2000). In our study heterozygous littermates (*Smn*^{+/-}; *SMN2*; *SMNΔ7*) were used as controls throughout. Between 3 and 7 animals were used per group; detailed numbers and ages of SMA animals used are listed in Tables 1 and 2. Transgenic

TABLE 2.

Number of SMA Mice and Control Littermates Used to Quantify Postsynaptic Pathology

Age (postnatal day)	Genotype	Muscle group	N		
			Mice	Muscles	Endplates
P5	Control	Extraocular	3	3	152
		Tongue	4	4	310
		Lumbricals	7	7	588
	SMA	Extraocular	3	3	118
		Tongue	5	5	408
		Lumbricals	3	3	189
P10	Control	Extraocular	4	5	188
		Tongue	5	5	463
		Lumbricals	7	7	479
	SMA	Extraocular	5	5	257
		Tongue	5	5	495
		Lumbricals	4	4	341
P14	Control	Extraocular	3	3	125
		Tongue	3	3	322
		Lumbricals	3	5	298
	SMA	Extraocular	3	4	269
		Tongue	4	4	413
		Lumbricals	3	5	355

TABLE 3.

Number of SOD1^{G93A} Mice and Control Littermates Used to Quantify Presynaptic Pathology

Age (postnatal day)	Genotype	Muscle group	N				
			Mice	Muscles	NMJs		
P56	Control	Extraocular	3	8	543		
		Lumbricals	4	15	990		
		Extraocular	3	7	419		
	SOD1 ^{G93A}	Lumbricals	4	15	1010		
		P84	Control	Extraocular	3	6	374
				Tongue	3	3	196
Lumbricals	4			12	978		
SOD1 ^{G93A}	Extraocular		4	7	453		
	Tongue		4	4	243		
	Lumbricals		4	16	1328		
P112	Control	Extraocular	4	6	375		
		Tongue	5	5	285		
		Lumbricals	5	18	1397		
	SOD1 ^{G93A}	Extraocular	4	5	317		
		Tongue	5	5	289		
		Lumbricals	3	10	819		
P133	Control	Extraocular	3	3	262		
		Tongue	4	4	206		
		Lumbricals	3	10	685		
	SOD1 ^{G93A}	Extraocular	3	4	296		
		Tongue	5	5	292		
		Lumbricals	3	8	516		

SOD1^{G93A} mice (B6.Cg-Tg(SOD1*G93A)1Gur/J; Jackson Laboratory Stock, Number 004435) were used as a model of ALS. These mice overexpress mutant human SOD1 protein leading to an ALS-like phenotype. Non-transgenic littermates were used as controls (Gurney et al., 1994). Between 3 and 9 animals were used per group; detailed numbers and ages of SOD1^{G93A} animals used are listed in Tables 3 and 4.

Muscle preparation

SOD1^{G93A} mice and control littermates (postnatal days P56–133) were sacrificed by inhalation of rising concentrations of CO₂. Neonatal SMNΔ7 SMA mice and control littermates (P5) were anesthetized by chilling on ice and killed by decapitation. P10 and P14 mice were sacrificed by intraperitoneal injection of avertin (tribromoethanol, Sigma, St. Louis, MO) at 0.5–0.6 mg/g body weight. The extraocular muscles (surrounding the eye), tongue, and lumbricals (from the plantar surface of the hind-paw) were dissected in 0.1M phosphate-buffered saline (PBS) and fixed in 4% paraformaldehyde (Sigma-Aldrich) for 10 minutes (extraocular and lumbricals) or 1 hour (tongue) at room temperature. All tongue muscles were cryoprotected in 20% sucrose in PBS and sectioned (30 μm). Extraocular and lumbrical muscles were dissected and stained whole-mount to allow for visualization of the entire innervation pattern, and detailed analysis of the neuromuscular junctions (Fig. 1) (Sleigh et al., 2014).

TABLE 4.
Number of SOD1^{G93A} Mice and Control Littermates Used to Quantify Postsynaptic Pathology

Age (postnatal day)	Genotype	Muscle group	N		
			Mice	Muscles	Endplates
P56	Control	Extraocular	3	10	354
		Lumbricals	4	15	459
	SOD1 ^{G93A}	Extraocular	3	7	239
		Lumbricals	5	19	565
P84	Control	Extraocular	3	10	369
		Tongue	3	3	291
		Lumbricals	4	11	347
	SOD1 ^{G93A}	Extraocular	4	13	549
		Tongue	4	4	384
		Lumbricals	4	14	489
P112	Control	Extraocular	5	17	472
		Tongue	5	5	437
		Lumbricals	9	27	1188
	SOD1 ^{G93A}	Extraocular	4	14	553
		Tongue	6	6	449
		Lumbricals	7	18	791
P133	Control	Extraocular	3	8	334
		Tongue	4	4	285
		Lumbricals	3	10	376
	SOD1 ^{G93A}	Extraocular	4	14	444
		Tongue	4	4	297
		Lumbricals	4	16	461

These muscles were gently stretched out laterally after dissection to optimize antibody penetration and increase visible muscle surface. For our analysis of the extraocular muscles we used the superior, medial, and inferior recti muscles, which are all innervated by axons projecting from the oculomotor nucleus in the brainstem. The medial rectus was omitted from this study as it is innervated instead by the abducens nerve. As the tongue was too large to allow for whole-mount the tissue was sectioned at 30 μ m thickness prior to staining.

Immunohistochemistry

Muscles were immunohistochemically processed to allow visualization of neuromuscular junctions. Neuromuscular junctions were labeled using established markers of presynaptic nerve terminals (neurofilament and synaptic vesicle protein) and postsynaptic motor

endplates (α -bungarotoxin, which binds to acetylcholine receptors on the muscle fibers). Specifically, tissues were permeabilized in Triton X-100 (Sigma; 0.1% neonatal extraocular and lumbrical muscles, 2% adult extraocular and lumbrical muscles, 4% all tongue tissue) and blocked in 10% donkey serum (Jackson ImmunoResearch, West Grove, PA) in 0.1M PBS for 1 hour at room temperature before incubation with primary antibodies directed against synaptic vesicle protein (SV2) (Buckley and Kelly, 1985) and neurofilament (2H3) (Dodd et al., 1988) overnight at 4°C. Further details of primary antibodies are listed in Table 5. After washing in 0.1% Triton X-100 and 10% donkey serum in 0.1M PBS for 1 hour at 4°C, muscles were incubated for 3 hours with Alexa Fluor 488 donkey antimouse secondary antibody in 0.1M PBS (1:500, Life Technologies, Bethesda, MD). Muscles were washed in 0.1M PBS for 30 min and then exposed to α -bungarotoxin (α -BTX) conjugated to tetramethyl-rhodamine isocyanate (TRITC; 1:1,000, Life Technologies) for 10 minutes to label postsynaptic acetylcholine receptors. Muscles were then whole-mounted in Mowiol 4-88 (Sigma-Aldrich) on glass slides and coverslipped for subsequent imaging.

Antibody characterization

We used a mouse monoclonal anti-Neurofilament (165 kDa) antibody from Developmental Studies Hybridoma Bank (DSHB, 2H3, Iowa City, IA), catalog number <http://dshb.biology.uiowa.edu/2H3>, antibody registry AB_2314897, at a concentration of 1:50. The immunogen used to generate the antibody was a membrane preparation obtained from embryonic day (E)14–E15 rat spinal cord tissue. A mouse monoclonal antisynaptic vesicle glycoprotein 2A (SV2A) from DSHB, catalog number <http://dshb.biology.uiowa.edu/synaptic-vesicles>, antibody registry ID AB_2315387 was used at a concentration of 1:100. The immunogen used to generate this antibody was purified synaptic vesicles. Omission of either primary or secondary antibodies did not result in significant background levels (Fig. 1M,N).

TABLE 5.
Antibodies Used for Immunohistochemistry

Name of antibody	Immunogen	Manufacturer	Catalog number	RRID	Clonality	Host species	Concentration
Neurofilament (165 kDa)	Membrane preparations obtained from E14–E15 rat spinal cord tissue	DSHB (2H3)	http://dshb.biology.uiowa.edu/2H3	AB_2314897	Monoclonal	Mouse	1:50
Synaptic vesicle glycoprotein 2A	Purified synaptic vesicles	DSHB (SV2)	http://dshb.biology.uiowa.edu/synaptic-vesicles	AB_2315387	Monoclonal	Mouse	1:100

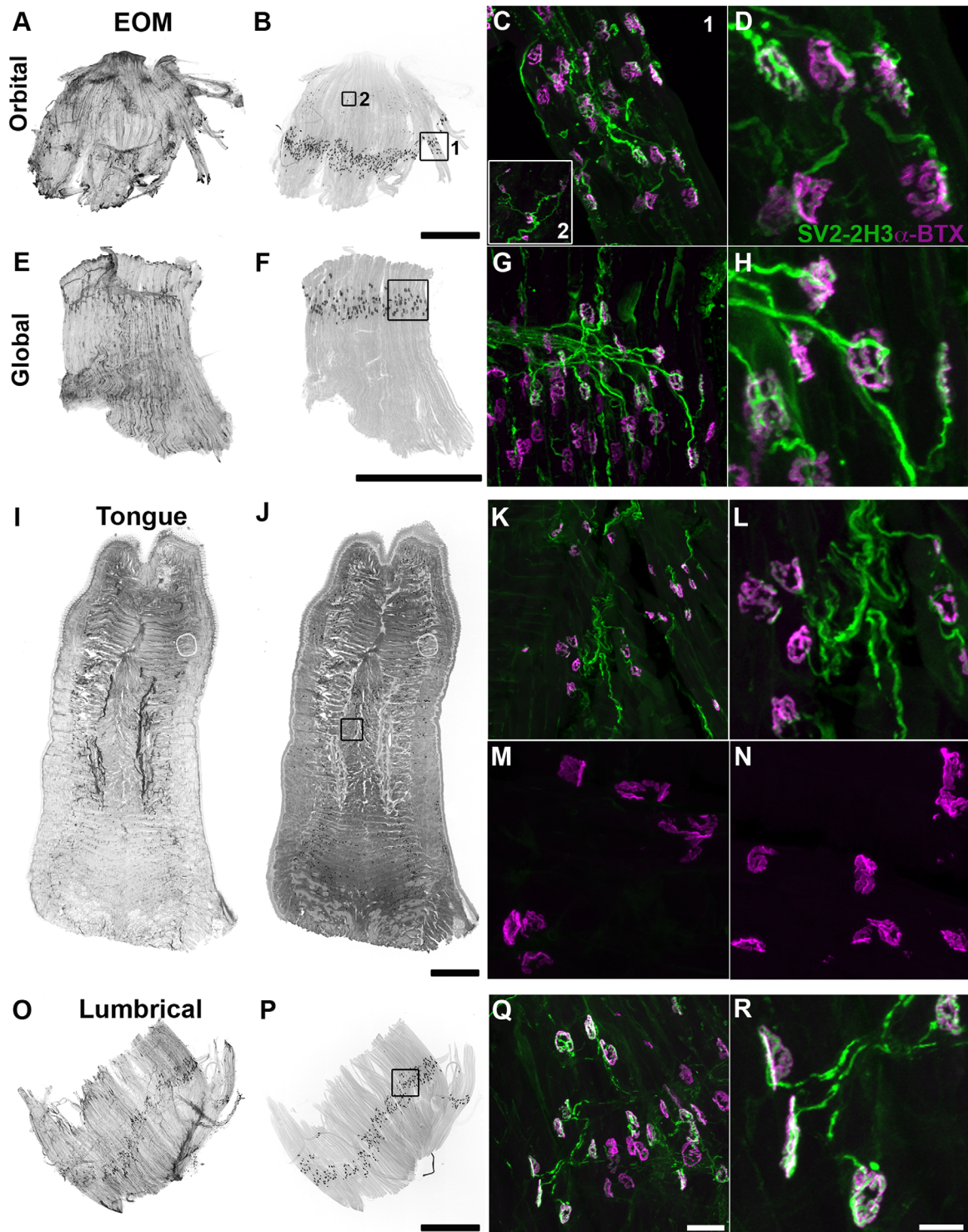


Figure 1. Morphology of muscle groups analyzed. Example confocal micrographs of muscles from a P84 wildtype mouse, stained with pre-synaptic markers 2H3 (neurofilament protein) and SV2 (synaptic vesicle protein 2) to label the incoming nerve terminal and α -bungarotoxin (α -BTX) to visualize the acetylcholine receptors on the postsynaptic muscle. Overview black and white images of both fluorescent channels of the whole muscles are provided, as well as high-magnification merges. Extraocular muscles analyzed included examples from both the orbital (A-D) and global (E-H) layers surrounding the eye. Montages shown are of whole-mount superior rectus muscles, showing the full innervation pattern (A,E) visualized with SV2 and 2H3 staining, and typical location of the endplate band (B,F) stained with α -BTX in both layers of muscle. Numerous examples of en-grappe endplates were seen in the orbital layer (inset 2 in C), but were not included in our analysis. Individual endplates are shown in the fluorescent merges (C,D,G,H; SV2 and 2H3 in green, α -BTX in magenta). I-L: Reconstructed montage of the innervation pattern of the tongue. As tongue muscles were too large to allow for whole-mount visualization, multiple 30- μ m thick sections were analyzed per muscle. As with the other muscle groups, the general pattern of innervation was remarkably conserved. M,N: Control immunostaining of tongue muscle. Omission of primary (M) or secondary (N) antibodies for neurofilament. Endplates were visualized with α -BTX. O-R: Whole-mount reconstruction of the first deep lumbrical muscle from the hind-paw, showing the typical innervation pattern (O) and endplates located in the center of each muscle fiber (P). All images shown here are representative of the morphology of the muscles analyzed in each group throughout this study. Scale bars = 500 μ m in B,F,J,P; 50 μ m in Q (applies to C,G,K); 20 μ m in R (applies to D,H,L,M,N).

Imaging and analysis

Muscle preparations were viewed using either a standard epifluorescence microscope (Zeiss Axio Imager M1 Upright microscope) or a laser scanning confocal microscope (Zeiss LSM700). Reconstructions of entire adult muscles from P84 wildtype animals for Figure 1 were performed using Zen software. Neuromuscular junctions (NMJs) from regions across the entire muscle were assessed in each preparation (detailed numbers are listed in Tables (1–4)). All analyses were performed blind to the genetic status of the material. For presynaptic analyses of extraocular, tongue, and lumbrical muscles, endplates were categorized as vacant (no neurofilament overlying the endplate), partially occupied (neurofilament overlying up to 80% of the endplate), or fully occupied (neurofilament overlying more than 80% of the endplate). For postsynaptic measurements each α -bungarotoxin-labeled motor endplate was manually outlined using ImageJ software (NIH, Bethesda, MD), which calculated total areas. Neonatal endplate maturity was analyzed by counting the number of perforations per endplate (areas without α -bungarotoxin staining within the perimeter of an endplate). All analyses were performed on en-face endplates only, as well as on Z-stack throughout the NMJs.

Statistics

All data were collected and analyzed using two-way analysis of variance (ANOVA), followed by Tukey's post-hoc test, in GraphPad Prism software (San Diego, CA). All results are expressed as mean \pm SEM.

RESULTS

The three muscle groups analyzed showed a consistent pattern of innervation between mice

In this study we analyzed the neuromuscular junction in three muscle groups: the extraocular muscles (surrounding the eye), tongue, and lumbricals (from the plantar surface of the hind-paw; Fig. 1). We included both orbital and global layers of extraocular muscle when dissection allowed this, and saw a consistent pattern of innervation in all adult muscles analyzed (Fig. 1A–H). Muscle endplates were located in a dense band, with a second band of smaller en-grappe endplates distal to this (Fig. 1B–D). Multiple en-grappe endplates are found on \sim 20% of muscle fibers in extraocular muscles, highly unusually for mammals who characteristically have a 1:1 ratio of endplate to muscle in the adult (Dietert, 1965; Namba et al., 1968; Porter, 2002). They are typically small and are innervated by subgroups of oculomotor neurons (Buttner-Ennever et al., 2001). Due

to their small size and distinct innervation pattern, en-grappe endplates were omitted from all analyses. However, no examples of vacant or partially occupied en-grappe endplates were seen in any muscle preparations from either SMA or SOD1^{G93A} mice (data not shown). The exterior part of the tongue was used for analysis. Two longitudinal bands of endplates were repeatedly observed, one per lateral side (Fig. 1I–L). In between these bands, scattered endplates were present in mainly the medial and posterior region (Fig. 1J–L). Outside of the lateral bands, small clusters of endplates were observed, of which the individual endplates were consistently bigger in size compared to those in the main bands. To control for unspecific anti-SV2 and 2H3 NF antibody stainings, we conducted control experiments, omitting either primary (Fig. 1M) or secondary antibodies (Fig. 1N), shown here for tongue muscle, while visualizing endplates with α -BTX. These experiments showed clearly that the antibody stainings were specific. The lumbrical muscles are located between the toes of the hind-paw and are innervated by the tibial nerve, which projects from the lumbar and sacral spinal cord. In our whole mount preparations of the first to fourth lumbrical muscles we routinely observed the typical endplate band in the center of the muscle fibers (Fig. 1O–R) in all mice analyzed.

Presynaptic pathology in the SMN Δ 7 mouse model of SMA

Innervation of the extraocular and tongue muscles was preserved in SMA, whereas lumbrical muscles showed loss of innervation at endstage

We began our analysis of neuromuscular pathology by quantifying innervation of neuromuscular junctions in extraocular, tongue, and lumbrical muscles in SMA mice over time. Motor endplates were categorized as fully occupied, partially occupied, or vacant based on the percentage covered by overlying nerve terminal. The timepoints used for all SMA analyses were P5 (early-symptomatic; SMA have an impaired righting response when placed on their side), P10 (mid-symptomatic; SMA mice are significantly smaller than control littermates and loss of limb coordination can be seen), and P14 (late-symptomatic; SMA typically die at P15). Neither the extraocular muscles (Fig. 2A–G) nor the tongue (Fig. 2H–N) showed any significant denervation in SMA mice over time compared to control littermates, from early to late-symptomatic stages of disease (Fig. 2A–N; $P > 0.05$ for all timepoints in both muscle groups). However, by late-stage (P14) endplates in SMA lumbrical muscles had significant levels of denervation

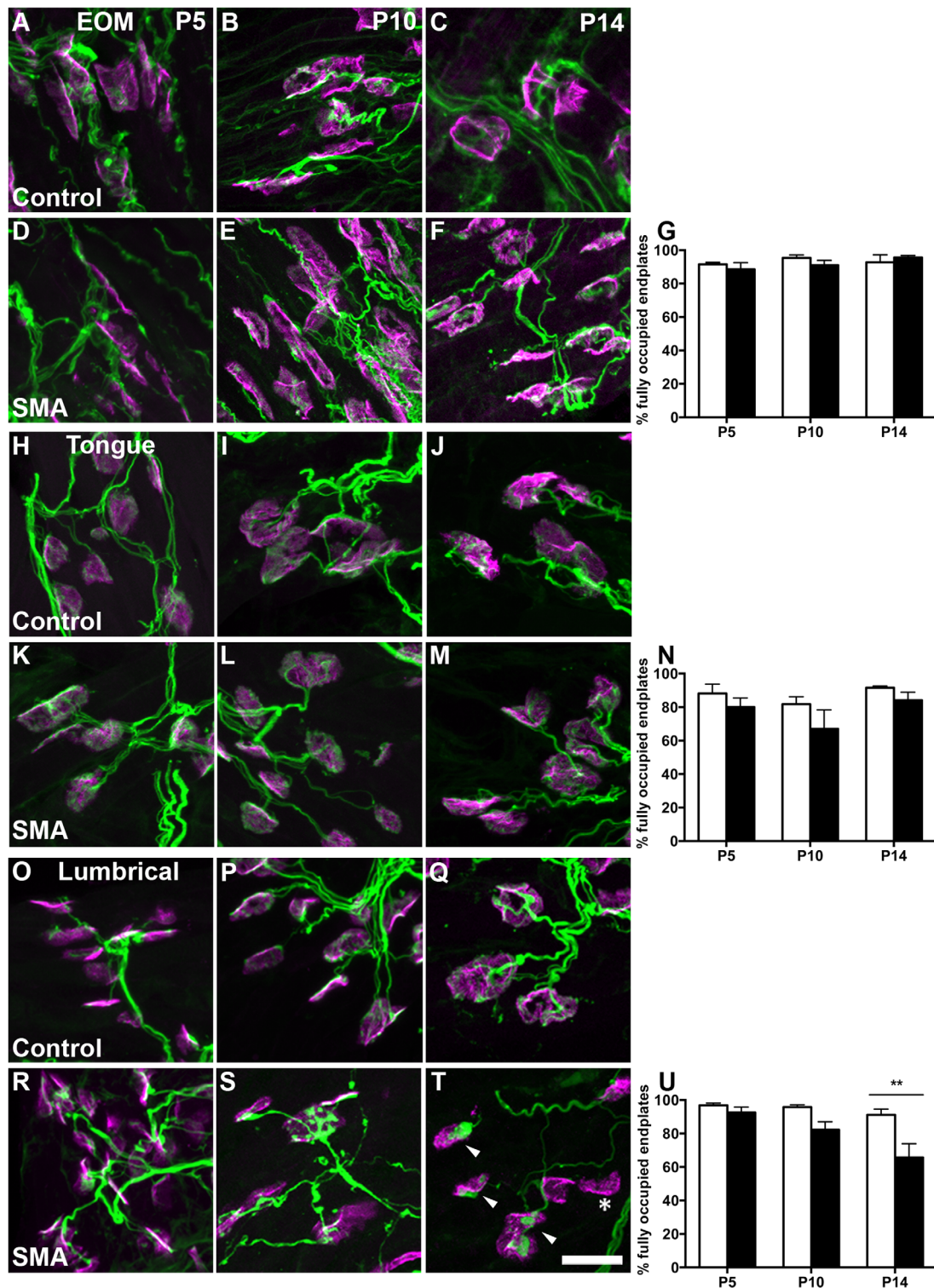


Figure 2. Analysis of presynaptic innervation of the neuromuscular junction in SMN Δ 7 SMA mice. **A–F:** Confocal micrographs showing representative images of neuromuscular junctions in extraocular muscles of SMA mice (D–F) and control littermates (A–C) at P5 (early-symptomatic; A,D), P10 (mid-symptomatic; B,E), and P14 (late-symptomatic; C,F), stained for 2H3, SV2 (green), and α -BTX (magenta). **G:** Bar graph showing percentages of fully occupied endplates in the extraocular muscles of control (white bars) and SMA (black bars) mice across time. There was no significant change in the levels of fully occupied endplates in mice of either genotype at P5, P10, or P14 ($P > 0.05$ for all timepoints). **H–M:** Confocal micrographs showing neuromuscular junctions in the tongue muscle of SMA mice (K–M) and control littermates (H–J) at P5 (H,K), P10 (I,L), or P14 (J,M). **N:** Neuromuscular junctions in the tongue muscles of SMA mice remained fully innervated throughout the time course of the disease, at levels comparable to those seen in control littermates ($P > 0.05$ for all timepoints). **O–T:** Confocal micrographs of neuromuscular junctions in the lumbrical muscles of SMA mice (R–T) and control littermates (O–Q) at P5 (O,R), P10 (P,S), or P14 (Q,T). Arrowheads indicate examples of partially innervated endplates and asterisks mark vacant endplates, seen in SMA muscle. **U:** By P14 (late-stage disease) lumbrical muscles in SMA mice showed a significant decrease in the percentage of fully occupied endplates compared to controls (P14 $P < 0.01$). At earlier timepoints there was no significant difference in levels of innervation between the genotypes (P5 and P10 $P > 0.05$). All bar graphs are mean \pm SEM; 2-way ANOVA with Tukey’s post-hoc test. White bars indicate control mice and black bars SMA mice throughout. $N =$ minimum of 3 mice per group. For details of total numbers of mice, muscles and neuromuscular junctions analyzed, see Table 1. Scale bar = 40 μ m in T (applies to all).

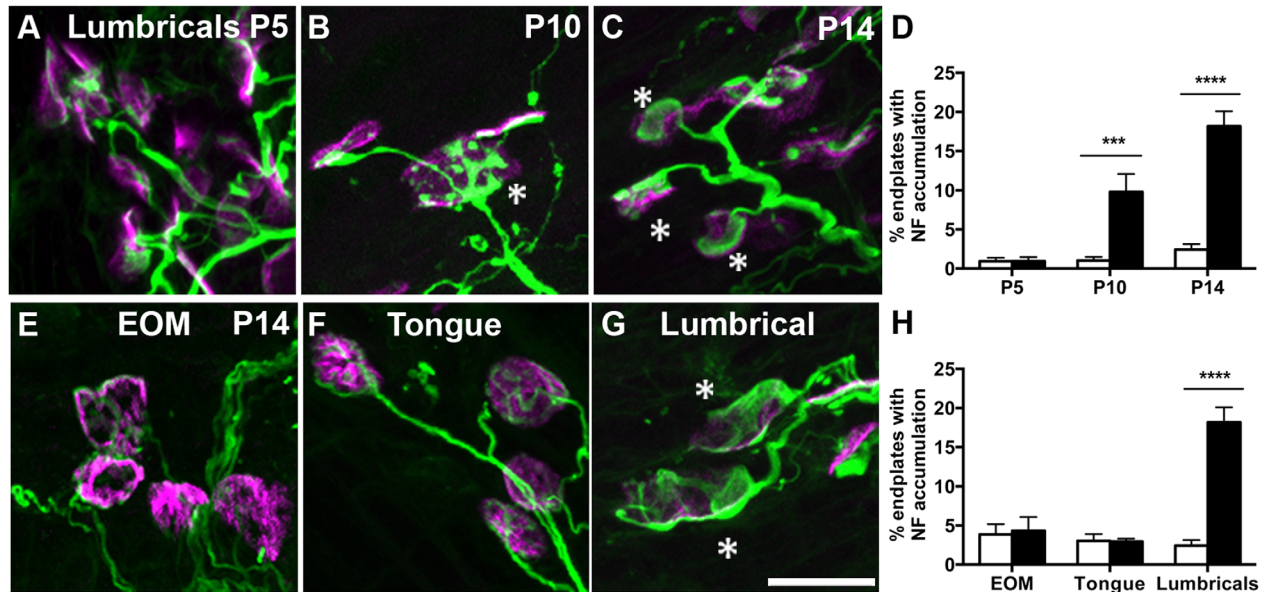


Figure 3. Neurofilament proteins accumulate presynaptically in lumbrical muscles, but not in extraocular or tongue muscles in SMN Δ 7 SMA mice. **A–C:** Confocal micrographs showing an increase in abnormal neurofilament accumulations in the presynaptic nerve terminals of neuromuscular junctions in SMA lumbrical muscles over time. Examples of accumulated neurofilament protein are marked by asterisks and can be seen at P10 (B) and P14 (C). **D:** The percentage of endplates with overlying neurofilament accumulation increased over time in the lumbrical muscles of SMA mice (black bars), compared to low levels (<2.5%) in control mice (white bars) at all timepoints (P5 $P > 0.05$; P10 $P < 0.001$; P14 $P < 0.0001$). **E–G:** Confocal micrographs showing extraocular (EOM; E) and tongue muscle (F) neuromuscular junction morphology at P14 with no evidence of neurofilament accumulation, compared to pathological neurofilament accumulation in the lumbrical muscles (G) at the same timepoint. Asterisks mark neuromuscular junctions with abnormal levels of neurofilament proteins. **H:** Quantification of neurofilament accumulation in P14 extraocular, tongue, and lumbrical muscles in control and SMA mice. Extraocular and tongue muscles from both control and SMA mice had very low levels of neurofilament accumulation, in contrast to the high levels in SMA lumbrical muscles at this timepoint (extraocular $P > 0.05$; tongue $P > 0.05$; lumbricals $P < 0.0001$). All muscles were stained for 2H3, SV2 (green) and α -BTX (magenta). Scale bar = 20 μ m in G (applies to all).

compared to control littermates (Fig. 2O–U; $P < 0.01$; asterisks in T indicate partially occupied endplates and arrowheads show vacant endplates).

Neurofilament proteins accumulated presynaptically in vulnerable lumbrical muscles, but not in extraocular or tongue muscles

While analyzing levels of denervation in the lumbrical muscles we noticed frequent incidences of presynaptic terminals with large accumulations of neurofilament protein. This has been shown to be a pathological feature of SMA in previous work on other mouse models of the disease (Cifuentes-Diaz et al., 2002; Kariya et al., 2008; Murray et al., 2008; Kong et al., 2009). In the lumbricals we found a significant increase in the percentage of neuromuscular junctions in SMA mice with neurofilament accumulations from P10 onwards (Fig. 3A–D). At the mid-symptomatic P10 timepoint, 9.8% of endplates analyzed in SMA lumbricals displayed accumulations of neurofilament, compared to just 1% in control littermates (Fig. 3B,D; $P < 0.001$). By late-stage of

the disease (P14) 18% of endplates analyzed in SMA lumbrical muscles had large neurofilament accumulations in their presynaptic terminals (Fig. 3C,D; $P < 0.0001$). We next assessed levels of neurofilament accumulation in the extraocular and tongue muscles. Even at P14 there was no increase in neurofilament in extraocular or tongue presynaptic terminals, in contrast to the lumbricals (Fig. 3E–H; extraocular $P > 0.05$, tongue $P > 0.05$, lumbricals $P < 0.0001$). Our results indicate that the presynaptic apparatus of the neuromuscular junction remains unchanged in extraocular and tongue muscles in SMA mice even at endstage, whereas pathological features such as denervation and neurofilament accumulation can be found in the lumbrical muscles from the mid-symptomatic stage onwards.

Postsynaptic pathology in the SMN Δ 7 mouse model of SMA

Decreased endplate area and maturity in lumbrical muscles as a consequence of SMA

We next measured the area of postsynaptic endplates on the muscle fibers of SMA mice and control

littermates. At the early (P5) and mid-symptomatic (P10) timepoints there was no difference in the size of endplates in the extraocular muscles in SMA mice (Fig. 4A,B,D,E,G; P5 $P > 0.05$, P10 $P > 0.05$). However, by endstage (P14) endplates in the SMA extraocular muscles were significantly smaller than those in control littermates (Fig. 4C,F,G; P14 $P < 0.01$). This appeared to be due to a failure of SMA endplates to increase in size between P5 and P14, whereas control endplates were significantly larger at P14 than P5, leading to the difference seen between the genotypes (Fig. 4H; control P5–P14 $P < 0.05$, SMA P5–P14 $P > 0.05$). In the tongue muscle there was no increase in size of endplates observed across time between P5 and P14 in either SMA or control mice (Fig. 4H–N). Consequently, there was no difference in endplate area between the two genotypes at any of the timepoints studied (Fig. 4N; $P > 0.05$ for all timepoints). In lumbrical muscles we observed an increase in endplate area across time in both control and SMA mice (Fig. 4O–Q, U; control P5–P14 $P < 0.0001$, Fig. 4R–U; SMA P5–P14 $P < 0.01$). However, while endplates in control muscles increased in size by 78.6% between P5 and P14 (from $79.8 \mu\text{m}^2$ to $142.5 \mu\text{m}^2$), those in SMA muscles only had a 39.2% increase in size in the same time frame (from $73.0 \mu\text{m}^2$ to $101.6 \mu\text{m}^2$). This translated to a significant difference in endplate area in SMA lumbrical muscles compared to control from P10 onwards (Fig. 4U; P5 $P > 0.05$, P10 $P < 0.05$, P14 $P < 0.0001$). As endplates mature they increase both in size and in sophistication of morphology (Sanes and Lichtman, 2001; Kong et al., 2009). To measure this we quantified the number of perforations in endplates in endstage (P14) extraocular, tongue, and lumbrical muscles in SMA and control mice. There was no difference in the percentage of endplates with perforations in SMA mice in either extraocular or tongue muscles compared to controls at this timepoint (Fig. 5A–C; extraocular $P > 0.05$, tongue $P > 0.05$). In contrast, there was a huge decrease in the percentage of endplates with perforations in the lumbrical muscles, from 57.0% in controls to just 8.4% in SMA mice (Fig. 5A–C; lumbricals $P < 0.0001$), indicating a simplified morphology and a reduction of maturity in this muscle. Quantification of percentage of endplates with perforations alone may underestimate the pathology in SMA due to the potential for multiple perforations per endplate as they mature (Fig. 5A). We therefore counted the total number of perforations per endplate in control and SMA mice (Fig. 5C–E) and calculated the average number of perforations per endplate at P14 across our three muscle groups (Fig. 5C). Once again, we saw no difference in the extraocular or tongue muscles in the SMA mice,

but a decrease in average number of perforations in lumbrical endplates from 0.84 in control mice to 0.10 in SMA (Fig. 5C; extraocular $P > 0.05$, tongue $P > 0.05$, lumbricals $P < 0.0001$).

Presynaptic pathology in the SOD1^{G93A} mouse model of ALS

The pattern of selective vulnerability of lumbrical muscles was conserved in ALS

In order to compare pathology and the selective resistance of the extraocular muscles across diseases, we next turned our attention towards the SOD1^{G93A} mouse model of ALS. As with the SMA mice, we began by quantifying presynaptic innervation of the same three muscle groups across time. Here we used P56 and P84 as early-stage timepoints, P112 as mid-stage, and P133 as late-stage. SOD1^{G93A} mice show clinical symptoms from P85, a loss of spinal motor neurons at P100, and a life span of ~ 160 days. Recapitulating the pattern seen in SMA, there was no change in the level of presynaptic innervation in the extraocular muscles of SOD1^{G93A} mice (Figs. 6A–H, 7A,B). This was reflected by a constant, high level of fully occupied endplates (Figs. 6A–H, 7A), accompanied by a low percentage (0–4.9%) of partially occupied endplates, which increased slightly during disease progression ($P < 0.01$, Fig. 7B). Tongue muscles also remained highly innervated, with no significant difference in fully occupied endplates between SOD1^{G93A} mice and control littermates across the timepoints measured (Figs. 6I–N, 7C). However, in SOD1^{G93A} mice the percentage of fully occupied endplates was significantly lower at P133 compared to P84 ($P < 0.01$). The number of partially occupied endplates was increased at P112 in SOD1^{G93A} mice compared to control littermates ($P < 0.01$, Fig. 7D), but not at P133. The lack of an increase of partial occupancy at P133 is likely a reflection of the variability in disease progression stage among the mice, as animals show a range in life-span from P155–P180. This was reflected by the large span in percentage of partially occupied (10–35%) endplates at this timepoint. A similar spread was observed for fully occupied endplates (44–90%), possibly explaining the lack of difference between SOD1^{G93A} and control mice at P133.

In contrast to the extraocular and tongue muscles, the lumbrical muscles in SOD1^{G93A} mice already had a profound decrease in the level of innervation by P84 (Figs. 6O,P,S,T, 7C; P84 $P < 0.001$), which persisted through both further timepoints analyzed (Figs. 6Q,R,U,V, 7E; P112 $P < 0.001$, P133 $P < 0.001$). However, the percentage of fully occupied neuromuscular junctions remained similar throughout the remainder of

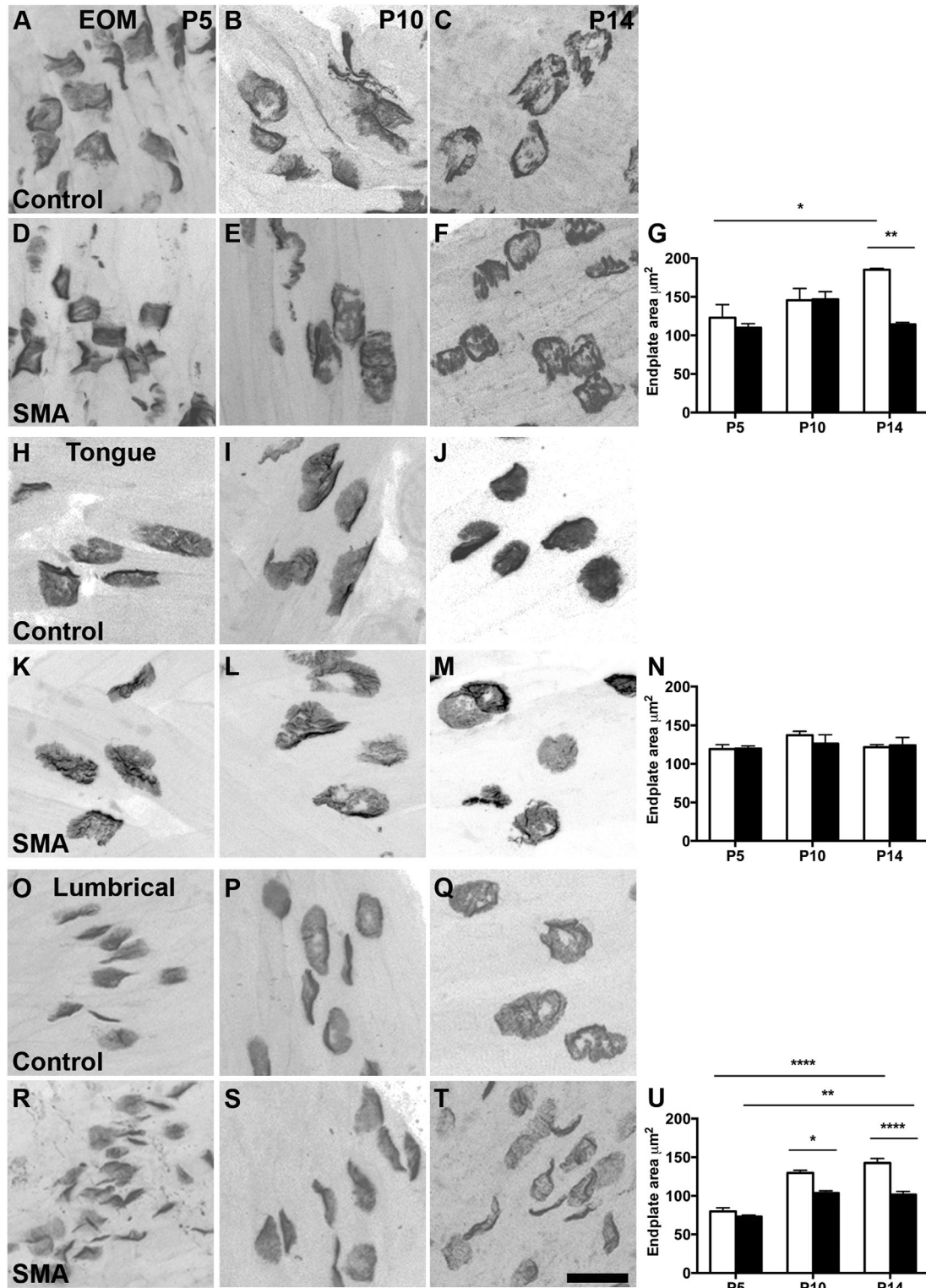


Figure 4. Analysis of postsynaptic endplate area in $SMN\Delta 7$ SMA mice. **A–F:** Representative black and white confocal micrographs showing images of endplates in extraocular muscles of SMA mice (D–F) and control littermates (A–C) at P5 (A,D), P10 (B,E), and P14 (C,F), stained with α -BTX. **G:** Bar graph showing endplate area increasing in the extraocular muscles of control mice across time (white bars; control P5–P14 $P < 0.05$) without equivalent growth in SMA endplates over time (black bars; SMA P5–P14 $P > 0.05$). By P14 there was therefore a significant difference in endplate size between the two genotypes (P14 $P < 0.01$). **H–M:** Confocal micrographs muscle endplates in the tongue muscle of SMA mice (K–M) and control littermates (H–J) at P5 (H,K), P10 (I,L), or P14 (J,M). **N:** Endplates in the tongue muscle remained similar in size between P5 and P14 in both SMA and control muscles ($P > 0.05$ for all timepoints). **O–T:** Confocal micrographs of muscle endplates in the lumbrical muscles of SMA mice (R–T) and control littermates (O–Q) at P5 (O,R), P10 (P,S), or P14 (Q,T), showing smaller and misshapen endplates in SMA muscles from P10 onwards. **U:** Despite an increase in SMA endplate areas between P5 and P14 (black bars; SMA P5–P14 $P < 0.01$), growth here was stunted compared to control littermates (white bars; control P5–P14 $P < 0.0001$), resulting in decreased endplate area in SMA lumbricals compared to controls from P10 onwards (P5 $P > 0.05$; P10 $P < 0.05$; P14 $P < 0.0001$). For details of total numbers of mice, muscles and endplates analyzed, see Table 2. Scale bar = 40 μ m in T (applies to all).

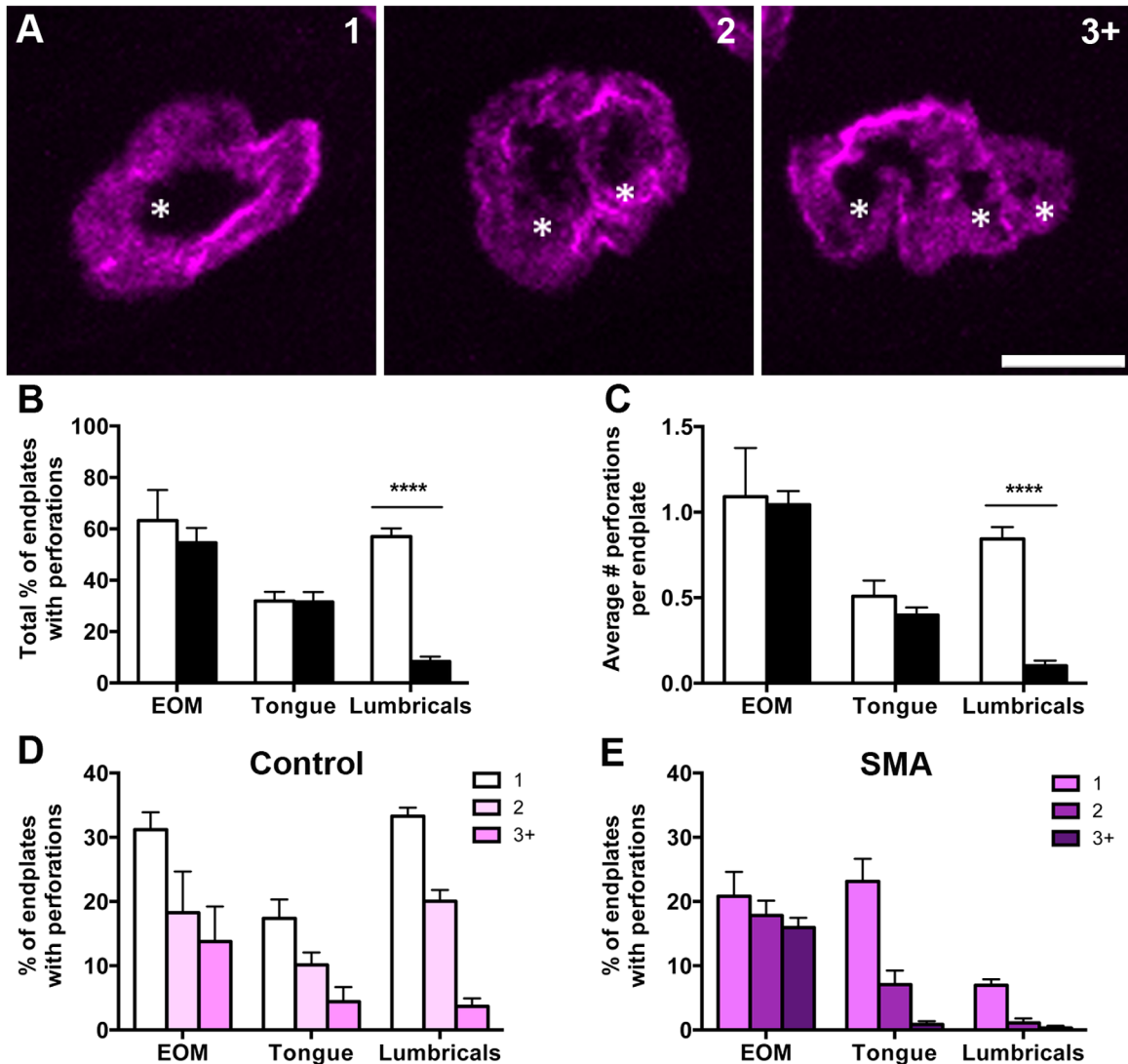


Figure 5. Decreased maturity of postsynaptic endplates in lumbrical muscles in SMA mice. **A:** Confocal micrographs showing example images of endplates from a control lumbrical muscle, with one, two, and three perforations, denoted by asterisks. **B:** Bar graph showing the percentage of endplates with any examples of perforations in extraocular (EOM), tongue, and lumbrical muscles in SMA and control mice at P14. No difference was seen in either extraocular or tongue muscles ($P > 0.05$ for both), but there was a significant decrease in the percentage of endplates with perforations in SMA lumbrical muscles ($P < 0.0001$). **C:** Bar graph showing the average number of perforations per endplate at P14 across the three muscle groups. Once again, no difference was seen in the extraocular or tongue muscles in the SMA mice, but there was a significant decrease in the average number of perforations in lumbrical endplates in SMA (extraocular $P > 0.05$; tongue $P > 0.05$; lumbricals $P < 0.0001$). **D,E:** Bar graphs showing the percentage of endplates in control (D) and SMA (E) mice with one, two, or more than three perforations. Scale bar = 10 μm in A.

the disease time course (Fig. 7E, P84: 67.2%, P112: 63.6%, P133: 64.5%), despite a worsening of the clinical phenotype in $\text{SOD1}^{\text{G93A}}$ mice between these timepoints. We hypothesize that this could be due to an increase in the levels of reinnervation in this muscle, leading to newly innervated neuromuscular junctions in the later timepoints. This is supported by a significant increase in the percentage of partially occupied endplates seen at the later timepoints of P112 and P133 (Fig. 7F; P112 $P < 0.01$, P133 $P < 0.01$). While these reinnervated end-

plates appear anatomically formed, they may not yet be fully functional, thus leading to the worsening phenotype in $\text{SOD1}^{\text{G93A}}$ mice despite regenerative responses. The pattern of preserved presynaptic innervation in the extraocular muscles and tongue and denervation of the lumbrical muscles in ALS parallels that seen in SMA. In contrast, no neurofilament accumulation was seen in any muscles from the $\text{SOD1}^{\text{G93A}}$ mice, unlike in SMA, where it is present from mid-symptomatic stages in vulnerable muscle groups (unpubl. obs.).

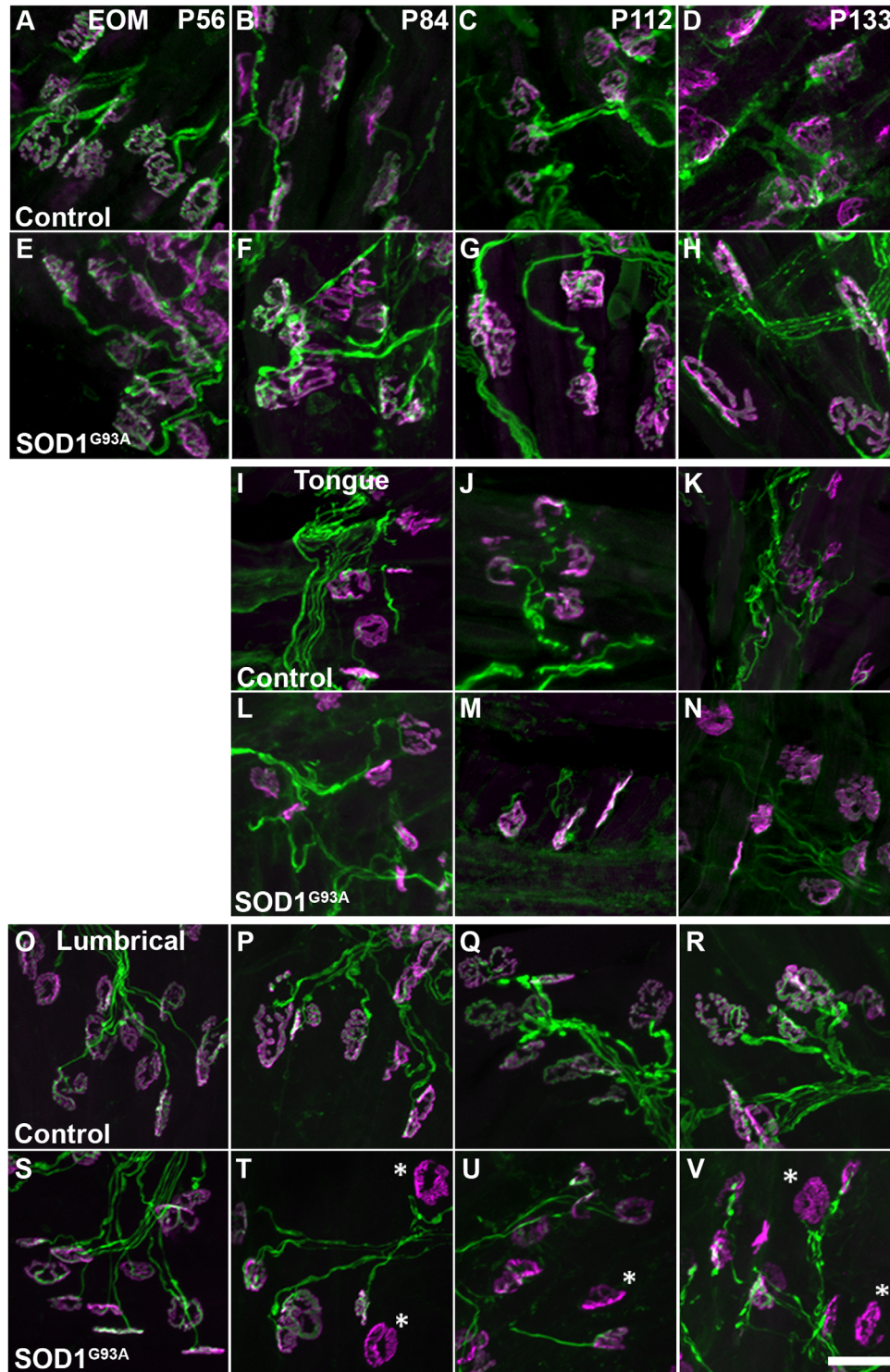


Figure 6. Presynaptic innervation of neuromuscular junctions in SOD1^{G93A} ALS mice. **A–H:** Confocal micrographs showing representative images of neuromuscular junctions in extraocular muscles of SOD1^{G93A} mice (E–H) and control littermates (A–D) at P56 (A,E), P84 (pre-symptomatic; B,F), P112 (mid-symptomatic; C,G), and P133 (late-symptomatic; D,H). **I–N:** Confocal micrographs of neuromuscular junctions in the tongue muscle of SOD1^{G93A} mice (L–N) and control littermates (I–K) at P84 (I,L), P112 (J,M), and P133 (K,N). **O–V:** Confocal micrographs of neuromuscular junctions in the lumbrical muscles of SOD1^{G93A} mice (S–V) and control littermates (O–R), showing vacant endplates (indicated by asterisks) in SOD1^{G93A} muscle from P84 onwards. All muscles were stained for 2H3, SV2 (green) and α -BTX (magenta). Scale bar = 40 μ m in V (applies to all).

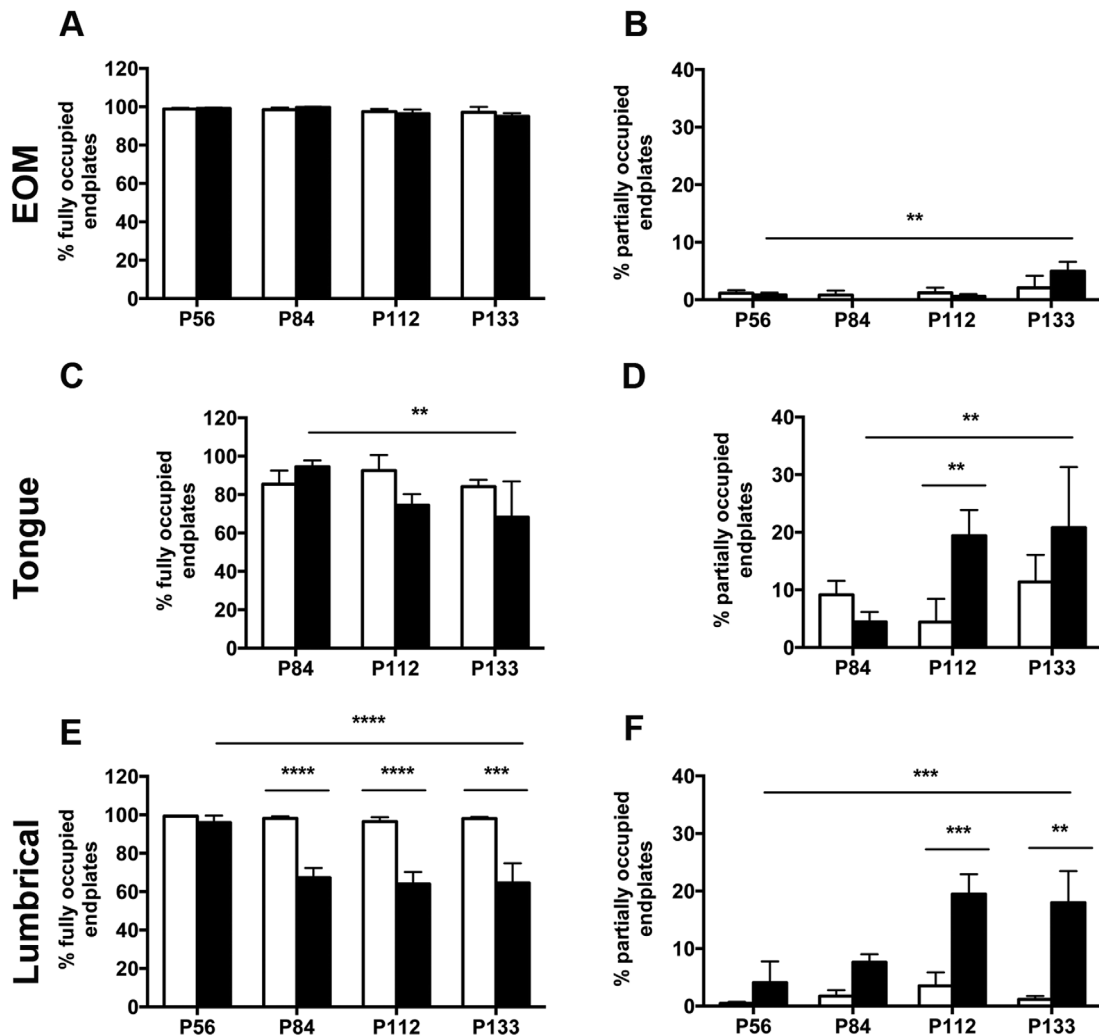


Figure 7. Quantification of presynaptic innervation of the neuromuscular junction in $SOD1^{G93A}$ ALS mice. **A:** Bar graph depicting percentages of fully occupied endplates in the extraocular muscles of control (white bars) and $SOD1^{G93A}$ (black bars) mice across time. There was no significant change in the levels of fully occupied endplates in $SOD1^{G93A}$ mice at any timepoint ($P > 0.05$ for all timepoints). **B:** Quantification of partially occupied endplates in extraocular muscle. No difference between $SOD1^{G93A}$ mice and controls is observed at any timepoint, although partial occupancy does increase in ALS mice from P84 to P133 ($P < 0.01$). **C:** Neuromuscular junctions in the tongue muscles of $SOD1^{G93A}$ mice remained fully innervated up until P133, at levels comparable to those seen in control mice at all timepoints ($P > 0.05$ for all timepoints). **D:** Partial occupancy of neuromuscular junctions in the tongue. The level of partial occupancy was higher in $SOD1^{G93A}$ mice compared to controls at P112 ($P < 0.01$) but not at P133. Overall, $SOD1^{G93A}$ mice display increasing levels of partial occupancy from P84 to P133 ($P < 0.01$). **E:** The percentage of fully occupied endplates in lumbrical muscles was significantly reduced in $SOD1^{G93A}$ mice from P84 onwards (P84 $P < 0.001$; P112 $P < 0.001$; P133 $P < 0.001$). **F:** Incidences of partially occupied endplates were increased in $SOD1^{G93A}$ lumbricals compared to controls at P112 ($P < 0.001$) and P133 ($P < 0.01$). In the ALS mice, the number of partially occupied endplates increased from P56 to P133 ($P < 0.001$). $N =$ minimum of 3 mice per group. For details of total numbers of mice, muscles and neuromuscular junctions analyzed, see Table 3.

Postsynaptic pathology in the $SOD1^{G93A}$ mouse model of ALS

Endplate area was significantly decreased in lumbrical muscles in ALS

Finally, we measured the area of postsynaptic endplates on the muscle fibers of $SOD1^{G93A}$ mice across the same range of timepoints. Corresponding to the lack of presynaptic pathology in extraocular and tongue muscle groups, in these mice we saw no alteration in endplate area in

either of these muscles, even at late-stage disease (Figs. 8A–N, 9A,B). In contrast, endplates in $SOD1^{G93A}$ lumbrical muscles were significantly smaller than those in their control counterparts from P112 onwards (Figs. 8O–V, 9C; P112 $P < 0.01$, P133 $P < 0.001$).

DISCUSSION

This article provides a detailed analysis of pathology at the neuromuscular junction across muscle groups in

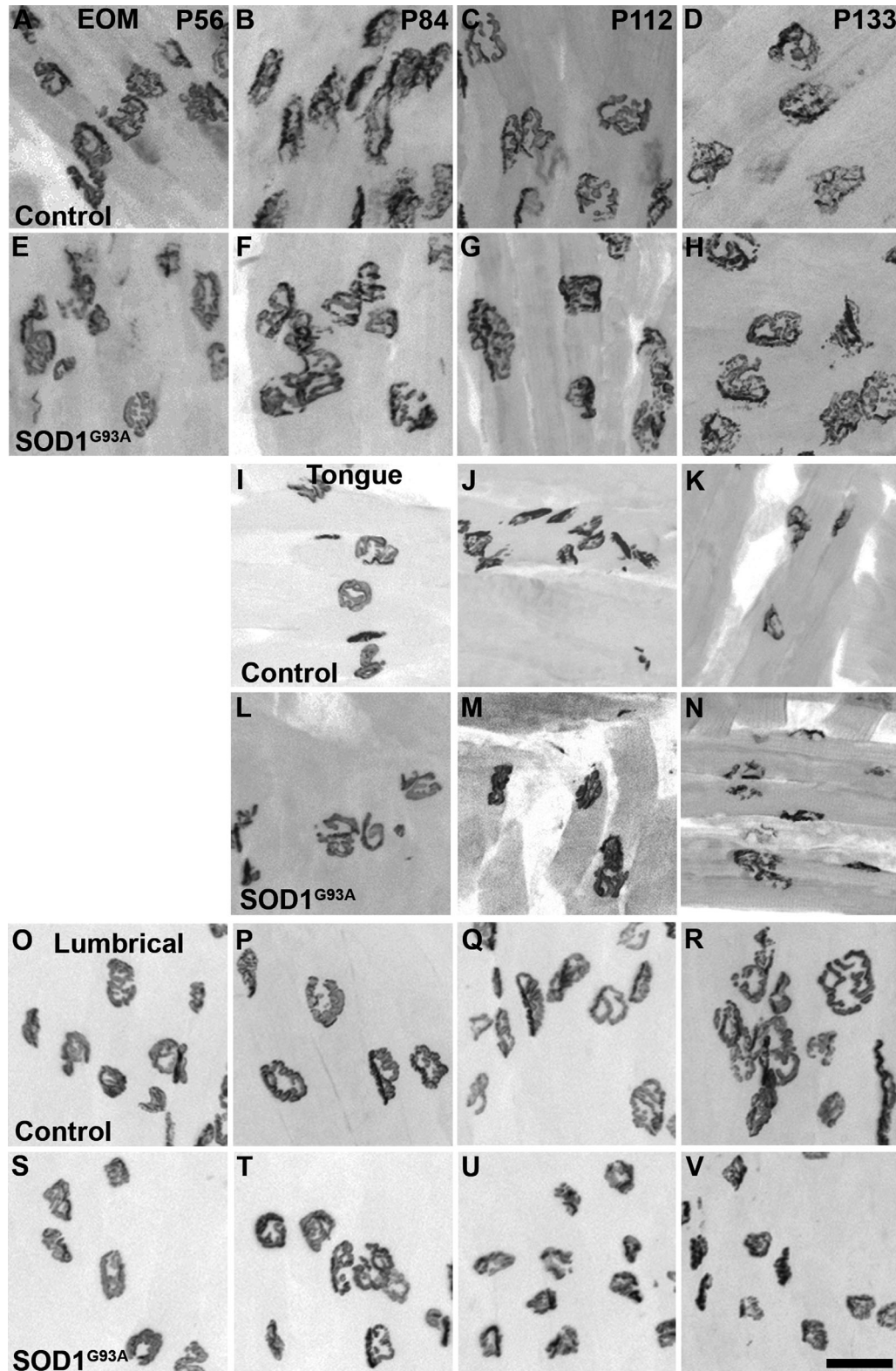


Figure 8. Postsynaptic endplate areas in SOD1^{G93A} ALS mice. **A–H:** Representative black and white confocal micrographs of endplates in extraocular muscles of SOD1^{G93A} mice (E–H) and control littermates (A–D) at P56 (A,E), P84 (B,F), P112 (C,G) and P133 (D,H), stained with α -BTX. **I–N:** Confocal micrographs of endplates in tongue muscle of SOD1^{G93A} mice (L–N) and control littermates (I–K) at P84 (I,L), P112 (J,M), and P133 (K,N). Endplates in the tongue were much smaller than those in other muscle groups examined. **O–V:** Confocal micrographs of muscle endplates in the lumbrical muscles of SOD1^{G93A} mice (S–V) and control littermates (O–R), showing smaller endplates in SOD1^{G93A} muscles from P112 onwards. For details of total numbers of mice, muscles and endplates analyzed, see Table 4. Scale bar = 40 μ m in V (applies to all).

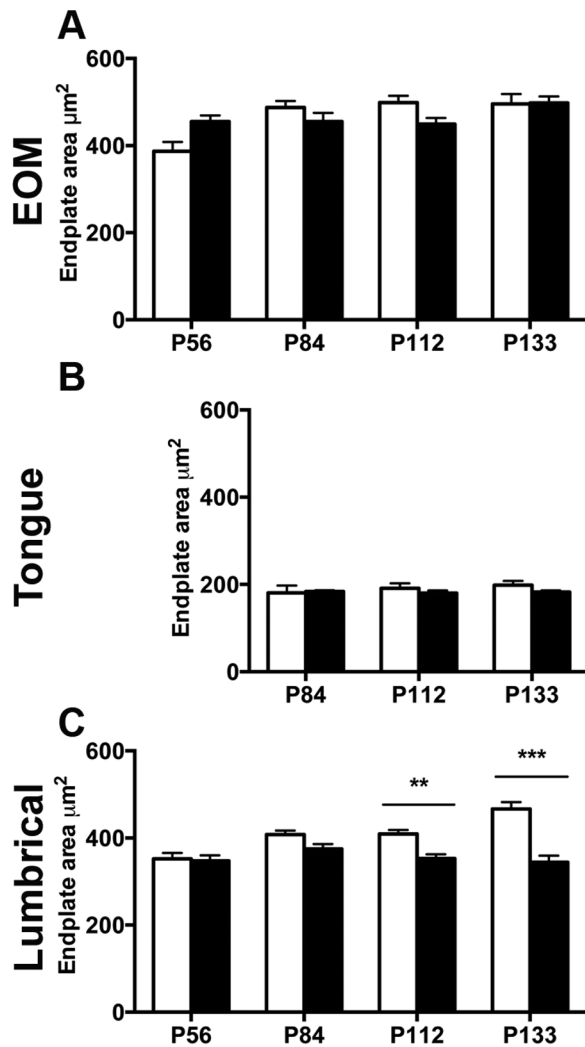


Figure 9. Quantification of postsynaptic endplate area in SOD1^{G93A} ALS mice. **A:** Bar graph showing no change in endplate area across time or between extraocular muscles of SOD1^{G93A} mice (black bars) and control mice (white bars) ($P > 0.05$ for all timepoints). **B:** No change was observed in endplate area of tongue neuromuscular junctions at any timepoint between SOD1^{G93A} mice and controls ($P > 0.05$ for all timepoints). **C:** Endplates in SOD1^{G93A} lumbricals were significantly smaller in area than those in control mice at P112 and P133 (P56 and P84 $P > 0.05$; P112 $P < 0.01$; P133 $P < 0.001$). $N =$ minimum of 3 mice per group. For details of total numbers of mice, muscles and neuromuscular junctions analyzed, see Table 4.

two different mouse models of motor neuron disease. In the SMN Δ 7 model of SMA we have shown that the lumbrical muscles of the hind-paw display a loss of neuronal innervation in late-stage mice, with pathological inclusions of neurofilament aggregating at the nerve terminals prior to any loss of connection. This muscle also displays a reduction in both the size and sophistication of the motor endplates on the muscle fibers. In contrast, there was no evidence of presynaptic pathology

in either the extraocular or tongue muscles in SMA mice, and postsynaptic endplates appeared similarly mature in SMA and control animals. In the SOD1^{G93A} mouse model presynaptic pathology in the lumbrical muscles was evident from an early-symptomatic timepoint, with no equivalent loss of innervation apparent in either the extraocular or tongue muscles. From mid-symptomatic onwards postsynaptic endplates in lumbricals were smaller in ALS animals but remained unchanged in other muscle groups. Thus, the pattern of selective vulnerability was conserved across these two mouse models of motor neuron disease. However, the first evidence of neuromuscular pathology occurred at different timepoints of disease progression, with much earlier evidence of presynaptic involvement in ALS, progressing to changes on the postsynaptic side. Conversely, in SMA changes appeared concomitantly at the neuromuscular junction, suggesting a dissociation of pre- and postsynaptic pathology in this disease.

Neuromuscular pathology in SMN Δ 7 SMA mice

Here we report the first evidence of sparing of ocular-motor neuromuscular junctions in the extraocular muscles in SMA. The relative resistance of this muscle group, even at endstage disease, is very much in agreement with clinical studies of SMA patients, where eye movement appears spared (Kubota et al., 2000). In contrast, the lack of involvement of the hypoglossal motor neurons innervating the tongue is in direct contradiction to clinical reports of tongue fasciculations (Iannaccone et al., 1993) and bulbar involvement leading to feeding and swallowing problems in patients. To our knowledge there have been no previous investigations into pathology of the tongue muscle in SMA animal models, but other muscles of mastication and swallowing were found to be denervated at endstage disease in the SMN Δ 7 model of SMA (Ling et al., 2012).

Our analysis of the three muscle groups showed that the neuromuscular junctions of lumbrical muscles were selectively vulnerable in both ALS and SMA. However, denervation occurred very late even in this vulnerable muscle group in SMA mice (P14) compared to the visible clinical phenotype, which is already evident at P6. This is in agreement with previous studies using the SMN Δ 7 model of SMA, which have shown only modest levels of denervation in other muscles compared to more severe models of SMA (Cifuentes-Diaz et al., 2002; Kariya et al., 2008; Murray et al., 2008; Kong et al., 2009). A more accurate measure of pathology at the neuromuscular junction in SMA mice is the accumulation of neurofilament proteins either in the

preterminal axon or in the nerve terminal itself (Cifuentes-Diaz et al., 2002). Using this measure we saw significant pathology at the P10 timepoint in the lumbricals, while even at endstage the extraocular muscles and tongue remained unaffected. This points to a high level of resistance in these muscle groups in this SMA mouse model, as neurofilament accumulation is a relatively early pathological presynaptic feature.

In addition to the presynaptic changes seen in the lumbrical muscles, this group also displayed morphological changes postsynaptically that appeared pathological. Endplates in SMA mice were smaller than those in their control counterparts from P10 onwards, preceding any presynaptic denervation and coinciding with significant levels of neurofilament accumulation. They also appeared misshapen and less mature, with fewer perforations indicating a slower switch from the neonatal plaque-like configuration to the adult pretzel morphology. This is an agreement with previous studies on other vulnerable muscle groups (Kong et al., 2009). Endplate maturation has been linked to a switch in acetylcholine receptor subunit expression from a γ - to an ϵ -subunit (Yumoto et al., 2005), which has been shown to be delayed in the severely affected intercostal and paraspinous muscles, but not in the relatively resistant diaphragm in SMA (Kong et al., 2009). This remains to be investigated in light of the differential vulnerability seen in the muscle groups studied here.

The smaller endplate area of SMA extraocular muscles at late-stage disease puzzled us initially, as this was the only evidence of any pathology in this muscle group. Additionally, other than their smaller size, endplates appeared morphologically normal, unlike those in the lumbrical muscles. We therefore hypothesize that the difference in size between control and SMA endplates in the extraocular muscles at the P14 timepoint was due to the lack of myofiber growth in the SMA mice, rather than a pathological shrinkage of this muscle group. Indeed, endplate and myofiber size were shown to be correlated during growth (Balice-Gordon and Lichtman, 1990). Moreover, SMA mice in our colony are significantly smaller than their control littermates by P6, and by P10 have a 48% reduction in overall body weight (colony records, data not shown). Stunted myofiber growth has also been reported before in the SMN Δ 7 model of SMA, although not in the muscle groups analyzed here (Le et al., 2005; Kong et al., 2009; Lee et al., 2011). This failure to grow continues until endstage disease, and it is therefore reasonable to assume that muscle groups that would usually be gaining in mass and size of muscle fibers during this postnatal period were smaller in the SMA animals, and thus gave rise to smaller endplate areas. In the tongue, mus-

cle endplates do not increase in area between P5 and P14 even in control animals, and thus no difference in size is seen in the SMA mice. In fact, tongue muscles appear to have small endplate areas even in adulthood; tongue endplates from control mice in our SOD1^{G93A} colony are less than half the size of those in extraocular or lumbrical muscles.

Neuromuscular pathology in SOD1^{G93A} ALS mice

We see the same pattern of lumbrical vulnerability and relative resistance of extraocular and tongue muscles repeated in the SOD1^{G93A} mouse model of ALS. The sparing of extraocular muscle seen here is in agreement with previous reports showing no loss of presynaptic innervation even at endstage in these mice (Tjust et al., 2012; Valdez et al., 2012). Several studies have documented an early degeneration of corticospinal motor neurons in the SOD1^{G93A} mouse (Ozdinler et al., 2011; Jara et al., 2012; Yasvoina et al., 2013). These findings clearly demonstrate that not only spinal and lower brainstem motor neurons are vulnerable in this ALS model, but also upper motor neurons, thus strengthening the finding of relative oculomotor neuron resistance. Valdez and colleagues also reported a sparing of this muscle group in aging, when muscles in the hindlimb, trunk, and neck are all susceptible to age-related structural changes (Tjust et al., 2012; Valdez et al., 2012).

Hypoglossal motor neuron somas have been shown to already be affected in 90-day-old mice, with a 12% cell loss at this stage and 28% at endstage of disease (Haenggeli and Kato, 2002). While in our analysis the percentage of fully occupied endplates did not differ between control and SOD1^{G93A} mice within each timepoint, the SOD1^{G93A} mice showed a progressive decrease of fully occupied endplates over time. The lack of difference between control and ALS mice likely reflects the large variability in disease stage of SOD1 mice at the timepoints analyzed.

One explanation for this apparent discrepancy between a larger central motor neuron loss with a milder peripheral NMJ pathology could be that motor neurons of the hypoglossal nucleus display regenerative properties and that such events mask the ongoing degeneration. Indeed, it has been shown that hypoglossal motor neurons display a high level of synaptic sprouting in the SOD1^{G93A} mouse, as indicated by their increased uptake and retrograde transport of muscle-injected adenoviruses (Millecamps et al., 2001). A high percentage of partially occupied endplates can indicate a regenerative phenotype in a muscle, as endplates are vacated and then reinnervated, passing through a

partially occupied state. In accordance with this, we found that the percentage of partially occupied endplates increased with disease in the tongue of SOD1^{G93A} mice. Within timepoints a significant difference in partial occupation between control and SOD1^{G93A} animals was observed at P112. However, no significant difference was observed at P133, again likely resulting from the large variability in disease stages of mice of the same age, particularly visible at the later timepoints.

In contrast to the extraocular and tongue muscles, lumbrical muscles were highly denervated prior to the onset of visible clinical symptoms in SOD1^{G93A} mice. The level of denervation did not appear to progress between pre-symptomatic and late-symptomatic stages, despite an obviously worsened phenotype in the mice. This is likely due to reinnervation, which occurs during disease progression (Bjornskov et al., 1984; Frey et al., 2000; Fischer et al., 2004; Schaefer et al., 2005), and is reflected in the increase in partially occupied endplates seen in this muscle group in our study.

Cross-disease comparison of ALS and SMA

Our analysis demonstrates that in ALS presynaptic pathology in lumbricals precedes any morphological changes at the endplate; in SMA evidence of pre- and postsynaptic pathology appear simultaneously. This indicates that mechanisms of neuromuscular disruption are distinct in these diseases. Our results in the SOD1^{G93A} mouse are consistent with the model of selective death of motor neurons in ALS, leaving disused muscle fibers, which therefore atrophy and shrink, giving rise to smaller motor endplates. Indeed, reduction of mutant SOD1 in motor neurons delayed onset and early progression of disease (Boillee et al., 2006), and motor neuron-specific expression of mutant SOD1 was sufficient to cause motor neuron degeneration and induce an ALS-like phenotype (Jaarsma et al., 2008).

Our observation of a simultaneous emergence of pre- and postsynaptic alterations in the lumbricals in SMA mice (at the mid-symptomatic P10 timepoint) indicates that low levels of SMN protein affect both motor nerves and muscle cells. However, recent genetic studies indicate that muscle does not require high levels of SMN protein, as muscle-specific removal of *Smn* in the SMN Δ 7 mouse had no phenotypic effect (Iyer et al., 2015). This would rather place the motor neuron as a driver of disease in SMA, even though visible muscle pathology appears simultaneously with presynaptic motor neuron loss. Indeed, it was recently shown that high SMN expression within motor neurons is required to maintain proper electrophysiological properties (McGovern et al., 2015).

Patterns of selective resistance and vulnerability

The results reported here provide new evidence for the relative resistance of the oculomotor neurons and their extraocular muscle targets in SMA, and add to the reports of conserved innervation of this muscle group in ALS mice (Tjust et al., 2012; Valdez et al., 2012). A key question in the field of motor neuron disease research currently is what causes some neuromuscular junctions to be resistant to disease triggers, while others are highly sensitive to the same genetic changes. Previous work has shown that this group of motor neurons has a distinct transcriptional profile and protein signature compared to other motor neuron groups, which could be underpinning their resistant properties (Hedlund et al., 2010; Brockington et al., 2013; Comley et al., 2015). Further investigation into the unique properties of these resistant motor neurons may provide new clues allowing for the development of therapeutic strategies to protect the vulnerable neuromuscular system.

ACKNOWLEDGMENT

We thank S. Cullheim for many helpful discussions and for critically reading the article.

CONFLICT OF INTEREST

The authors identify no conflicts of interest in this study.

ROLE OF AUTHORS

All authors had full access to all the data in the study and take responsibility for the integrity of the data and the accuracy of the data analysis. Study concept and design: LHC and EH. Acquisition of data: LHC, JN, JFN, and EH. Analysis and interpretation of data: LHC, JN, JFN, and EH. Drafting of the article: LHC and EH. Critical revision of the article for important intellectual content: JN. Statistical analysis: LHC, JN, JFN, and EH. Obtained funding: EH. Study supervision: EH.

LITERATURE CITED

- Al-Chalabi A, Jones A, Troakes C, King A, Al-Sarraj S, van den Berg LH. 2012. The genetics and neuropathology of amyotrophic lateral sclerosis. *Acta Neuropathol* 124: 339–352.
- Balice-Gordon RJ, Lichtman JW. 1990. In vivo visualization of the growth of pre- and postsynaptic elements of neuromuscular junctions in the mouse. *J Neurosci* 10:894–908.
- Bjornskov EK, Norris FH Jr, Mower-Kuby J. 1984. Quantitative axon terminal and end-plate morphology in amyotrophic lateral sclerosis. *Arch Neurol* 41:527–530.
- Boillee S, Yamanaka K, Lobsiger CS, Copeland NG, Jenkins NA, Kassiotis G, Kollias G, Cleveland DW. 2006. Onset

- and progression in inherited ALS determined by motor neurons and microglia. *Science* 312:1389–1392.
- Brockington A, Ning K, Heath PR, Wood E, Kirby J, Fusi N, Lawrence N, Wharton SB, Ince PG, Shaw PJ. 2013. Unravelling the enigma of selective vulnerability in neurodegeneration: motor neurons resistant to degeneration in ALS show distinct gene expression characteristics and decreased susceptibility to excitotoxicity. *Acta Neuropathol* 125:95–109.
- Bruneteau G, Bauche S, Gonzalez de Aguilar JL, Brochier G, Mandjee N, Tanguy ML, Hussain G, Behin A, Khiami F, Sariali E, Hell-Remy C, Salachas F, Pradat PF, Lacomblez L, Nicole S, Fontaine B, Fardeau M, Loeffler JP, Meininger V, Fournier E, Koenig J, Hantai D. 2015. Endplate denervation correlates with Nogo-A muscle expression in amyotrophic lateral sclerosis patients. *Ann Clin Transl Neurol* 2:362–372.
- Buckley K, Kelly RB. 1985. Identification of a transmembrane glycoprotein specific for secretory vesicles of neural and endocrine cells. *J Cell Biol* 100:1284–1294.
- Buttner-Ennever JA, Horn AK, Scherberger H, D'Ascanio P. 2001. Motoneurons of twitch and nontwitch extraocular muscle fibers in the abducens, trochlear, and oculomotor nuclei of monkeys. *J Comp Neurol* 438:318–335.
- Cifuentes-Diaz C, Nicole S, Velasco ME, Borra-Cebrian C, Panozzo C, Frugier T, Millet G, Roblot N, Joshi V, Melki J. 2002. Neurofilament accumulation at the motor endplate and lack of axonal sprouting in a spinal muscular atrophy mouse model. *Hum Mol Genet* 11:1439–1447.
- Comley L, Allodi I, Nichterwitz S, Nizzardo M, Simone C, Corti S, Hedlund E. 2015. Motor neurons with differential vulnerability to degeneration show distinct protein signatures in health and ALS. *Neuroscience* 291:216–229.
- Coovert DD, Le TT, McAndrew PE, Strasswimmer J, Crawford TO, Mendell JR, Coulson SE, Androphy EJ, Prior TW, Burghes AH. 1997. The survival motor neuron protein in spinal muscular atrophy. *Hum Mol Genet* 6:1205–1214.
- Dengler R, Konstanzer A, Kuther G, Hesse S, Wolf W, Struppler A. 1990. Amyotrophic lateral sclerosis: macro-EMG and twitch forces of single motor units. *Muscle Nerve* 13:545–550.
- Dietert SE. 1965. The demonstration of different types of muscle fibers in human extraocular muscle fibers in human extraocular muscle by electron microscopy and cholinesterase staining. *Invest Ophthalmol* 4:51–63.
- Dodd J, Morton SB, Karagogeos D, Yamamoto M, Jessell TM. 1988. Spatial regulation of axonal glycoprotein expression on subsets of embryonic spinal neurons. *Neuron* 1:105–116.
- Faravelli I, Nizzardo M, Comi GP, Corti S. 2015. Spinal muscular atrophy—recent therapeutic advances for an old challenge. *Nat Rev Neurol* 11:351–359.
- Fischer LR, Culver DG, Tennant P, Davis AA, Wang M, Castellano-Sanchez A, Khan J, Polak MA, Glass JD. 2004. Amyotrophic lateral sclerosis is a distal axonopathy: evidence in mice and man. *Exp Neurol* 185:232–240.
- Frey D, Schneider C, Xu L, Borg J, Spooren W, Caroni P. 2000. Early and selective loss of neuromuscular synapse subtypes with low sprouting competence in motoneuron diseases. *J Neurosci* 20:2534–2542.
- Gizzi M, DiRocco A, Sivak M, Cohen B. 1992. Ocular motor function in motor neuron disease. *Neurology* 42:1037–1046.
- Gurney ME, Pu H, Chiu AY, Dal Canto MC, Polchow CY, Alexander DD, Caliendo J, Hentati A, Kwon YW, Deng HX, et al. 1994. Motor neuron degeneration in mice that express a human Cu,Zn superoxide dismutase mutation. *Science* 264:1772–1775.
- Haenggeli C, Kato AC. 2002. Differential vulnerability of cranial motoneurons in mouse models with motor neuron degeneration. *Neurosci Lett* 335:39–43.
- Hedlund E, Karlsson M, Osborn T, Ludwig W, Isacson O. 2010. Global gene expression profiling of somatic motor neuron populations with different vulnerability identify molecules and pathways of degeneration and protection. *Brain* 133:2313–2330.
- Iannaccone ST, Browne RH, Samaha FJ, Buncher CR. 1993. Prospective study of spinal muscular atrophy before age 6 years. DCN/SMA Group. *Pediatr Neurol* 9:187–193.
- Iyer CC, McGovern VL, Murray JD, Gombash SE, Zaworski PG, Foust KD, Janssen PM, Burghes AH. 2015. Low levels of Survival Motor Neuron protein are sufficient for normal muscle function in the SMNDelta7 mouse model of SMA. *Hum Mol Genet* 24:6160–6173.
- Jaarsma D, Teuling E, Haasdijk ED, De Zeeuw CI, Hoogenraad CC. 2008. Neuron-specific expression of mutant superoxide dismutase is sufficient to induce amyotrophic lateral sclerosis in transgenic mice. *J Neurosci* 28:2075–2088.
- Jara JH, Villa SR, Khan NA, Bohn MC, Ozdinler PH. 2012. AAV2 mediated retrograde transduction of corticospinal motor neurons reveals initial and selective apical dendrite degeneration in ALS. *Neurobiol Dis* 47:174–183.
- Kariya S, Park GH, Maeno-Hikichi Y, Leykekhman O, Lutz C, Arkovitz MS, Landmesser LT, Monani UR. 2008. Reduced SMN protein impairs maturation of the neuromuscular junctions in mouse models of spinal muscular atrophy. *Hum Mol Genet* 17:2552–2569.
- Kong L, Wang X, Choe DW, Polley M, Burnett BG, Bosch-Marce M, Griffin JW, Rich MM, Sumner CJ. 2009. Impaired synaptic vesicle release and immaturity of neuromuscular junctions in spinal muscular atrophy mice. *J Neurosci* 29:842–851.
- Kubota M, Sakakihara Y, Uchiyama Y, Nara A, Nagata T, Nitta H, Ishimoto K, Oka A, Horio K, Yanagisawa M. 2000. New ocular movement detector system as a communication tool in ventilator-assisted Werdnig-Hoffmann disease. *Dev Med Child Neurol* 42:61–64.
- Le TT, Pham LT, Butchbach ME, Zhang HL, Monani UR, Coovert DD, Gavrilina TO, Xing L, Bassell GJ, Burghes AH. 2005. SMNDelta7, the major product of the centromeric survival motor neuron (SMN2) gene, extends survival in mice with spinal muscular atrophy and associates with full-length SMN. *Hum Mol Genet* 14:845–857.
- Lee YI, Mikesh M, Smith I, Rimer M, Thompson W. 2011. Muscles in a mouse model of spinal muscular atrophy show profound defects in neuromuscular development even in the absence of failure in neuromuscular transmission or loss of motor neurons. *Dev Biol* 356:432–444.
- Ling KK, Gibbs RM, Feng Z, Ko CP. 2012. Severe neuromuscular denervation of clinically relevant muscles in a mouse model of spinal muscular atrophy. *Hum Mol Genet* 21:185–195.
- Liu KX, Edwards B, Lee S, Finelli MJ, Davies B, Davies KE, Oliver PL. 2015. Neuron-specific antioxidant OXR1 extends survival of a mouse model of amyotrophic lateral sclerosis. *Brain* 138:1167–1181.
- Logroscino G, Traynor BJ, Hardiman O, Chio A, Mitchell D, Swingler RJ, Millul A, Benn E, Beghi E. 2010. Incidence of amyotrophic lateral sclerosis in Europe. *J Neurol Neurosurg Psychiatry* 81:385–390.
- Maselli RA, Wollman RL, Leung C, Distad B, Palombi S, Richman DP, Salazar-Gruesso EF, Roos RP. 1993. Neuromuscular transmission in amyotrophic lateral sclerosis. *Muscle Nerve* 16:1193–1203.
- McGovern VL, Iyer CC, Arnold WD, Gombash SE, Zaworski PG, Blatnik AJ 3rd, Foust KD, Burghes AH. 2015. SMN

- expression is required in motor neurons to rescue electrophysiological deficits in the SMN Δ 7 mouse model of SMA. *Hum Mol Genet* 24:5524–5541.
- Millicamps S, Nicolle D, Ceballos-Picot I, Mallet J, Barkats M. 2001. Synaptic sprouting increases the uptake capacities of motoneurons in amyotrophic lateral sclerosis mice. *Proc Natl Acad Sci U S A* 98:7582–7587.
- Monani UR, Sendtner M, Coovert DD, Parsons DW, Andreassi C, Le TT, Jablonka S, Schrank B, Rossoll W, Prior TW, Morris GE, Burghes AH. 2000. The human centromeric survival motor neuron gene (SMN2) rescues embryonic lethality in Smn(-/-) mice and results in a mouse with spinal muscular atrophy. *Hum Mol Genet* 9:333–339.
- Murray LM, Comley LH, Thomson D, Parkinson N, Talbot K, Gillingwater TH. 2008. Selective vulnerability of motor neurons and dissociation of pre- and postsynaptic pathology at the neuromuscular junction in mouse models of spinal muscular atrophy. *Hum Mol Genet* 17:949–962.
- Murray LM, Talbot K, Gillingwater TH. 2010. Review: neuromuscular synaptic vulnerability in motor neurone disease: amyotrophic lateral sclerosis and spinal muscular atrophy. *Neuropathol Appl Neurobiol* 36:133–156.
- Namba T, Nakamura T, Takahashi A, Grob D. 1968. Motor nerve endings in extraocular muscles. *J Comp Neurol* 134:385–396.
- Nimchinsky EA, Young WG, Yeung G, Shah RA, Gordon JW, Bloom FE, Morrison JH, Hof PR. 2000. Differential vulnerability of oculomotor, facial, and hypoglossal nuclei in G86R superoxide dismutase transgenic mice. *J Comp Neurol* 416:112–125.
- Ozdinler PH, Benn S, Yamamoto TH, Guzel M, Brown RH Jr, Macklis JD. 2011. Corticospinal motor neurons and related subcerebral projection neurons undergo early and specific neurodegeneration in hSOD1G(9)(3)A transgenic ALS mice. *J Neurosci* 31:4166–4177.
- Porter JD. 2002. Extraocular muscle: cellular adaptations for a diverse functional repertoire. *Ann N Y Acad Sci* 956:7–16.
- Renton AE, Chio A, Traynor BJ. 2014. State of play in amyotrophic lateral sclerosis genetics. *Nat Neurosci* 17:17–23.
- Sanes JR, Lichtman JW. 2001. Induction, assembly, maturation and maintenance of a postsynaptic apparatus. *Nat Rev Neurosci* 2:791–805.
- Schaefer AM, Sanes JR, Lichtman JW. 2005. A compensatory subpopulation of motor neurons in a mouse model of amyotrophic lateral sclerosis. *J Comp Neurol* 490:209–219.
- Sleigh JN, Burgess RW, Gillingwater TH, Cader MZ. 2014. Morphological analysis of neuromuscular junction development and degeneration in rodent lumbrical muscles. *J Neurosci Methods* 227:159–165.
- Spataro R, Ciriaco M, Manno C, La Bella V. 2014. The eye-tracking computer device for communication in amyotrophic lateral sclerosis. *Acta Neurol Scand* 130:40–45.
- Thomson SR, Nahon JE, Mutsaers CA, Thomson D, Hamilton G, Parson SH, Gillingwater TH. 2012. Morphological characteristics of motor neurons do not determine their relative susceptibility to degeneration in a mouse model of severe spinal muscular atrophy. *PLoS One* 7:e52605.
- Tjust AE, Brannstrom T, Pedrosa Domellof F. 2012. Unaffected motor endplate occupancy in eye muscles of ALS G93A mouse model. *Front Biosci (Schol Ed)* 4:1547–1555.
- Valdez G, Tapia JC, Lichtman JW, Fox MA, Sanes JR. 2012. Shared resistance to aging and ALS in neuromuscular junctions of specific muscles. *PLoS One* 7:e34640.
- Wirth B, Herz M, Wetter A, Moskau S, Hahnen E, Rudnik-Schoneborn S, Wienker T, Zerres K. 1999. Quantitative analysis of survival motor neuron copies: identification of subtle SMN1 mutations in patients with spinal muscular atrophy, genotype-phenotype correlation, and implications for genetic counseling. *Am J Hum Genet* 64:1340–1356.
- Wirth B, Brichta L, Schrank B, Lochmuller H, Blick S, Baasner A, Heller R. 2006. Mildly affected patients with spinal muscular atrophy are partially protected by an increased SMN2 copy number. *Hum Genet* 119:422–428.
- Yasvoina MV, Genc B, Jara JH, Sheets PL, Quinlan KA, Milosevic A, Shepherd GM, Heckman CJ, Ozdinler PH. 2013. eGFP expression under UCHL1 promoter genetically labels corticospinal motor neurons and a subpopulation of degeneration-resistant spinal motor neurons in an ALS mouse model. *J Neurosci* 33:7890–7904.
- Yumoto N, Wakatsuki S, Sehara-Fujisawa A. 2005. The acetylcholine receptor gamma-to-epsilon switch occurs in individual endplates. *Biochem Biophys Res Commun* 331:1522–1527.